Deep eutectic solvent electrolytes based on trifluoroacetamide and LiPF$_6$ for Li-metal batteries

Lorenzo Mezzomo[a], Nicolò Pianta[a], Irene Ostroman[a], Niv Aloni[b], Diana Golodnitsky[b], Emanuel Peled[b], Piercarlo Mustarelli[a,c]*, Riccardo Ruffo[a,c]

[a] Dipartimento di Scienza dei Materiali, Università di Milano Bicocca, 20125 Milano, Italy

[b] School of Chemistry, Tel Aviv University, 6997801, Tel Aviv, Israel

[c] National Reference Center for Electrochemical Energy Storage (GISEL) - Consorzio Interuniversitario Nazionale per la Scienza e Tecnologia dei Materiali (INSTM), 50121 Firenze, Italy

Abstract

New generation lithium batteries require better performances, improved safety, and sustainability. Better performances can be obtained with lithium anodes and high-voltage cathodes, which in turn pose more pressure on the electrolyte stability, which is mandatory for safety. Deep Eutectic Solvents (DESs) are promising components for safer and more environmentally sustainable electrolytes. We investigate the physico-chemical properties of DESs made with 2,2,2-trifluoroacetamide (TFA) and LiPF$_6$. The best composition is tested against Li metal and two cathode active materials: LiFePO$_4$ (LFP) and high voltage LiNi$_{1-x-y}$Mn$_x$Co$_y$O$_2$ (NMC). We obtain good electrochemical performance in a Li-metal cell with LFP. Accelerated rate calorimetry shows improved thermal stability of the Li |DES | NMC cell with respect to a commercial liquid electrolyte.

Keywords

Lithium metal batteries, electrolyte, accelerated rate calorimetry, deep eutectic solvents, LiPF$_6$

1. Introduction

Lithium rechargeable batteries are expected to play a fundamental role in the automotive and transport sectors as well as in residential storage applications [1–4]. At present, the market state-of-the-art (SoA) still consists of the 3a generation which uses graphite negative electrode, at most with small amounts of silicon, LiNi$_{0.33}$Mn$_{0.33}$Co$_{0.33}$O$_2$ (NMC111) positive electrode and organic-based liquid electrolytes (mainly carbonates) with additives [5–7]. Major improvements in the performance evolution of the next generation are expected to be related to the use of lithium metal at the anode and high-energy cathodes. Mixed oxides with layered structure of the family LiNi$_{1-x-y}$Mn$_x$Co$_y$O$_2$ where x=3, y=0.2 (NMC532); x=y=0.2 (NMC622); or x=y=0.1 (NMC811) are attracting particular interest due to the superior specific capacity [8]. These chemistries will require liquid electrolytes with wider electrochemical stability window [9] ($\sim$ 4.5 V vs. Li$^+$/Li) to fully exploit the higher specific capacity of the cathode. However, the Ni-rich NMC layered oxides suffer of thermal instability which is particularly critical for the device safety when they are coupled with flammable electrolytes, such as formulations based on mixtures of cyclic and linear carbonates. Indeed, in conditions of overcharging, overheating, or short-circuiting of a lithium-ion battery, during the ensuing thermal runaway, the cathode can release oxygen into the flammable electrolyte and cause the device to explode [9,10]. For these reasons, new electrolytes should assure better properties in terms of safety, no or low flammability, high current rate, sustainability, and cost [11,12]. Among the solutions reported in the recent literature to overcome these issues, an important role is played by liquid saline systems (molten salts) in the temperature range of use of the batteries, such as ionic liquids (ILs) and deep eutectic solvents (DESs) [13–15]. ILs were largely studied in the last years both in the liquid and the plastic crystal solid analogue

forms [16,17]. They have good safety properties, but are expensive, often difficult to synthesize, and characterized by high viscosity [18], which limits high power applications.

DESs are neoteric liquids generally obtained by the combination of a halide quaternary ammonium salt (e.g., choline chloride) with hydrogen-bond (HB) donors (e.g., amines, amides, urea, etc.) or metal salts (e.g., $LiPF_6$) able to assure HB-mediated self-association, to form a eutectic mixture with a melting point much lower than that of the individual components [19–21]. With respect to ILs, DESs have significant advantages, including higher biodegradability, lower cost and toxicity (choline chloride is a well-known chicken feed [22]), ease of preparation by temperature-assisted mixing without special purification procedures, possibility of calibrating the chemical-physical properties in a wide composition range [23,24]. DESs based on N-methylacetamide with different lithium salts [$LiN(CF_3SO_2)_2$, $LiPF_6$, $LiNO_3$] were suggested as electrolytes for lithium-ion batteries. However, these systems are liquid at room temperature only for low lithium content (Li molar fraction x < 0.35), which limits ionic conductivity to ~1 mS cm^{-1} [25]. Binary DES electrolytes based on methanesulfonamide and N,N-dimethyl methanesulfonamide with lithium bis(fluoro)sulfonimide, and lithium bis(trifluoromethane)sulfonimide were also reported [26]. Our group reported on bio-inspired choline-chloride-based DESs encompassing $LiN(CF_3SO_2)_2$ (LiTFSI) and $LiPF_6$ which showed room temperature conductivity exceeding 5 mS cm^{-1} [27]. Later, DESs were used to prepare solid or semi-solid electrolytes [28–30].

Recently, a new DES based on the use of LiTFSI and 2,2,2-trifluoroacetamide (TFA) was introduced as stable lithium electrolyte up to high voltage [31]. This system showed a conductivity of 1.5 mS cm^{-1} at 30°C and a quite unusual anodic stability, however the charge efficiencies of half cells equipped with $LiMn_2O_4$ were around 80%, despite of the use of carbonates as additives in the electrolytic mixture. It is therefore evident that a careful evaluation of TFA-based DESs has yet to be carried out and their practical application validated.

In this paper, we reported for the first time on a DES obtained by using 2,2,2-trifluoroacetamide (TFA) as the HBD, and LiPF$_6$ as HBA. This makes the system simpler to prepare, at the same time offering the possibility to explore a large composition range. We also explored the role of some additives to obtain better interfacial stability through the formation of a more stable solid electrolyte interface (SEI) [32]. In the following, the advantages of the use of the TFA-based electrolyte compared to the carbonate approach are firstly discussed, after which the chemical-physical characterization of DES is presented, reporting the thermal, electrical, and electrochemical properties. Preliminary results on the use of a TFA-based formulation in cells with lithium metal and LiFePO$_4$ and LiNi$_{0.33}$Mn$_{0.33}$C$_{0.33}$O$_2$ cathodes are presented. As proof of concept of the improved cell safety, we finally compared accelerating rate calorimetry (ARC) tests on cells equipped with NMC cathode and both the commercial and the DES electrolytes.

1. **Experimental section**

1.1 Materials

2,2,2-Trifluoroacetamide (TFA, 99%) was acquired from Fluorochem Ltd. (UK) and dried under vacuum for 2h before using. Lithium hexafluorophosphate (LiPF$_6$, battery grade), lithium bis(trifluoromethanesulfonyl)imide (LiTFSI, anhydrous 99.99%), 1.0 M LiPF$_6$ in EC/DMC=50/50 (LP30, battery grade), ethylene carbonate (EC, anhydrous 99%), fluoroethylene carbonate (FEC, anhydrous 99%), 1-methyl-2-pyrrolidinone (NMP, anhydrous 99.5%), and lithium nickel manganese cobalt oxide (LiNi$_{0.33}$Mn$_{0.33}$Co$_{0.33}$O$_2$, NMC111) were provided by Sigma Aldrich. PVdF 6020 was acquired by Solvay Specialty Polymers S.p.a. (Italy). Lithium iron phosphate was obtained by HydroQuebec (Canada). All the materials and the electrochemical cells were manipulated in Ar-filled glove boxes ([O$_2$], [H$_2$O] < 0.1 ppm).

2.2 Materials characterization

Karl-Fisher titration was performed on a Metrohm 899 Coulometer equipped with a generator electrode with diaphragm. Hydranal Coulomat AG and CG were used as reagents for anodic and cathodic compartments, respectively. The instrument was previously calibrated using Hydranal CRM Water Standard 1.0. About 0.2 ml of DESs were added in the anodic compartment and the analysis was carried on until the H_2O drift reached a value < 5.0 µg min^{-1}.

Thermogravimetric analysis (TGA) was carried out on a Mettler Toledo TGA/DSC1 STAR^e System (temperature range 30-500°C, heating rate of 10°C min^{-1} under constant N_2 flux of 50 mL min^{-1}) to evaluate the thermal stability of DESs.

Thermal properties were investigated using differential Scanning Calorimetry (DSC) on the same Mettler Toledo instrument sealing the samples into aluminum pans (volume of 40 µL). A sealed, empty pan was used as reference. All the analyses were performed using the following thermal protocol under N_2 flux of 80 mL min^{-1}: i) cooling the system down to -40°C at 1°C min^{-1}; ii) isotherm at -40°C for 30 minutes to induce crystallization; iii) further cooling down to -80°C at 1°C min^{-1}; iv) heating to 80°C at 5°C min^{-1} to observe the endothermic phenomena.

The morphology of the Li metal electrodes after stripping plating was characterized by the SEM Zeiss Gemini electron microscope on samples prepared as described below.

For the Inductively Coupled Plasma Optical Emission Spectroscopy (ICP-OES) measurements, 10 mg of active cathode materials (LFP and NMC532) have been suspended in 500 mg (approx. 294 mL) of LiPF$_6$:TFA 20:80 DES. After a week, the solution was filtered using PTFE filters (pore size: 0.45 µm) and 50 µL were taken and diluted in water so to obtain 10 mL of solution. Nitric acid was also added (2vv%). The instrument was the ICP_AES (Instruments SA, Jobin-Yvon 38 Sequential, France).

2.3 Electrical and Electrochemical Characterization

The ionic conductivity of all the samples was determined using Impedance Spectroscopy with an AMEL 192/K1 conductivity cell with two black platinum electrodes and a cell constant K=1.06 cm.

Transference numbers were evaluated by the Bruce Vincent method by using a Li|DES|Li CR2032 symmetrical coin cell and applying a constant voltage of 10 mV until observing a stabilization of the delivered current. Impedance spectra have been collected before and after the polarization.

The electrochemical stability window (ESW) of DESs was determined performing cyclic voltammetry (CV) with a scan rate of 1 mV s^{-1} and using three-electrode Swagelok cells with carbon-coated Al (for oxidation) or Cu (for reduction) as working (WE) electrode and Li foil disks as counter (CE) and reference (RE) electrodes. Potential range were set up to 5.5 V vs Li^+/Li for oxidation and down to -0.075V vs Li^+/Li for reduction testing.

Stripping-plating analyses were carried out on symmetric Li|DES|Li CR2032 symmetrical coin cells delivering an alternatively positive and negative constant current density of 1.0 mA cm^{-2} for 1 hour (lithium plating capacity =1 mAh cm^{-2}).

SEM images were collected to detect any difference between the surfaces of metallic lithium after cycling in presence of the DES electrolyte with and without additives. In order to do this, two coin cells with metallic lithium electrodes were assembled. A glass microfiber separator was soaked with the two electrolytes. Such cells were cycled for 10 cycles with a current density of 1 mA cm^{-2}, 2h per cycle. The cells were then opened in glove box, the electrodes were extensively washed in DMC so to remove the electrolyte remaining on the surface. Finally, the lithium electrodes were stored in vials, then transported to the SEM where they were rapidly transferred in the sample holder to avoid reactions with oxygen and water.

Swagelok^{TM} full cells were assembled having Li as CE and RE, and cathodic materials prepared as follows as WE. LiFePO$_4$ (LFP) and LiNi$_{0.33}$Mn$_{0.33}$Co$_{0.33}$O$_2$ (NMC111) based electrodes were obtained via doctor blading on Al foils of NMP based slurries with 80 wt% of active material, 10 wt% of

conductive SuperP^{TM} carbon black, and 10 wt% of PVdF 6020 as binder (active material loading ≈2mg cm^{-2}). The cells were cycled at a current rate equal to C/10. All the electrolytes were soaked on GF/B Glass Microfiber Whatman^{TM} Filter with an average loading of 150 μL for 16mm separator disks.

Accelerated Rate Calorimetry (ARC) tests were performed using an ES-ARC instrument (THT Ltd., UK). The thermal behaviour of two 2032-coin cells, assembled with metallic lithium as negative electrode, NMC532 (MTI electrode sheet, active mass loading: 12.1 mg cm^{-2}) as the positive electrode and LP30 or DES as the electrolyte was explored. The experimental procedure consists in heating steps of 5°C followed by 10 minutes to allow thermalization of the working chamber. After that, the instrument spends 10 minutes to evaluate any differences in the temperatures (i.e., exothermic processes) recorded by the four thermocouples. If no differences are measured, the temperature is increased again by 5°C and the step is repeated, otherwise the temperature is monitored for the entire exothermic process duration, only to be increased again when it is finished, up to a maximum temperature of 250°C.

3 Results and Discussion

3.1 Electrolytes preparation

The flammability of commercial carbonate-based electrolytes can be ascribed to linear molecules that are commonly used to decrease the solution viscosity due to the presence of ethylene carbonate (EC). Examples of such linear systems are diethyl carbonate (DEC) and dimethyl carbonate (DMC). Table 1 shows the chemical and physical characteristics of interest taken from the corresponding safety data sheets. Both DEC and DMC have low flash point and are classified "hazard 3" in flammability, i.e., can be ignited under almost all ambient temperature conditions. Other electrolyte solvents (such as EC) or SEI forming additives (fluoroethylene carbonate, FEC)

are much more stable and do not pose stringent safety concerns [33]. Thus, one of the main advantages of using a TFA-based DES, which is a solid powder at room temperature (melting point = 72.5°C), would be to avoid linear carbonates making the battery safer.

Table 1. Hazard level of some electrolyte solvents and additives in LIBs.

| | Flash point (°C) | Auto-ignition temperature (°C) | NFPA 704 rating | | |
			H	F	I
EC	150	-	2	1	0
DEC	25	445	1	3	1
DMC	16	465	0	3	0
FEC	102.2	-	2	0	0
TFA	-	-	2	1	0

NFPA=Standard System for the Identification of the Hazards of Materials for Emergency Response (National Fire Protection Association, US) H=Health; F=Flammability, I=instability-reactivity: the higher the number, the worse the performance.

As mentioned in the Introduction, the use of TFA as HBD in deep eutectic electrolytes has been already reported in the literature with LiTFSi as HBA [31]. Anyway, the cycling performance resulted not satisfying and the system showed poor conductivity. Consequently, we decided to investigate other Li salts as feasible HBA, and, among others, $LiPF_6$ resulted particularly promising. The TFA-based deep eutectic solvents were produced by mixing the desired amounts of HBD (TFA) and HBA ($LiPF_6$). Six different TFA:$LiPF_6$ compositions were explored with the TFA molar ratio ranging from 0.5 to 0.9 (see Table 2). To improve the dielectric properties and the electrochemical stability, two more electrolytes were prepared by adding non-flammable carbonates to the TFA:$LiPF_6$ 80:20 composition, which was proven to be the most conducting one.

Both the DES precursors, as shown in Figure 1a, appeared as white powders while their mixtures give a clear and homogenous liquid after mildly heating for 30 minutes and then stirring at room temperature overnight (Figure 1b). Only the solution with the higher TFA amount (TFA:$LiPF_6$ 90:10) showed some instability with secondary phase separation in contact with the glass walls, as

discussed later. Karl-Fisher titration was carried out on mixtures to determine the amount of H_2O contained into the DESs, and in all the cases, the amount of water was below 50 ppm. In particular, TFA:LiPF$_6$ 80:20 DES had a water content of 36.6 ppm, only slightly higher than the one of commercial carbonates. Anyway, the electrolyte is hygroscopic since the same analysis performed after 3h of exposition to open air yielded a result of 196 ppm.
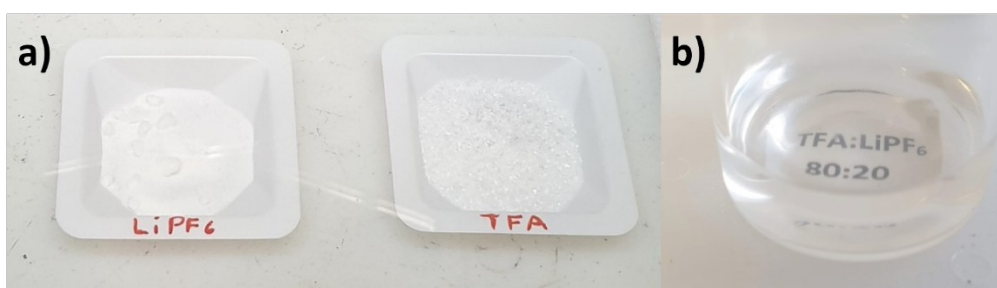

Figure 1. LiPF$_6$ and TFA powders in molar ratio 80:20 a) before and b) after the mixing.

Flammability testing has been also conducted to verify the safety improvements imparted by DES with respect to commercial carbonate electrolyte. In Figure S1 in the Supplementary Information it is possible to observe that the Celgard® H2010 separator supporting TFA:LiPF$_6$ 80:20 DES is mostly unaffected by a free flame for more than 15 seconds. Conversely, the polymeric separator soaked with LP30 was burned when subjected for 3 seconds to the same treatment.

Table 2. List of the investigated samples.

	Component 1	Component 2	Molar ratio	Additives wt%
TFA:LiPF$_6$ 50:50	TFA	LiPF$_6$	50:50	---
TFA:LiPF$_6$ 60:40	TFA	LiPF$_6$	60:40	---
TFA:LiPF$_6$ 70:30	TFA	LiPF$_6$	70:30	---
TFA:LiPF$_6$ 75:25	TFA	LiPF$_6$	75:25	---
TFA:LiPF$_6$ 80:20	TFA	LiPF$_6$	80:20	---
TFA:LiPF$_6$ 90:10	TFA	LiPF$_6$	90:10	---
TFA:LiPF$_6$ 80:20 +10%EC	TFA	LiPF$_6$	80:20	10% EC
TFA:LiPF$_6$ 80:20 +10%EC +5%FEC	TFA	LiPF$_6$	80:20	10% EC, 5% FEC

3.2 Electrolytes characterization

Differential scanning calorimetry was used to determine the phase diagram of the TFA:LiPF$_6$ binary system shown in Figure 2a. In the DSC curves (see Figure S2 in the Supplementary Information) the melting temperatures were estimated form the onset of the endothermic processes observed during the final heating ramp. The addition of LiPF$_6$ to pure TFA dramatically decreases the melting temperature, and the supposed eutectic composition (80:20) shows a eutectic temperature of 4°C. For all the solutions, the DSC thermograms also confirmed the presence of a sharp glass transition followed by an enthalpy endothermic overshoot, typical of similar systems [34,35], usually connected to kinetic structural rearrangement in the viscous liquid state at T>T$_g$=[-70°C; -65°C].

Thermogravimetric analysis (TGA) confirmed that the TFA:LiPF$_6$ 80:20 DES is thermally stable up to T>100°C (Figure 2b). Conversely, pristine TFA powder, which presents a melting point T$_m$≈70°C and a boiling point T$_b$≈165°C, started to decompose at slightly lower temperature (≈100°C). It is also worth noticing that all the solutions with a molar ratio different from the eutectic composition displayed a somehow bimodal weight loss profile attributable to the degradation of two different phases present in the system.

To further evaluate the thermal stability of these compounds, 1st order derivative of the previously reported TGA curves was computed to extract the derivative thermogravimetric profiles and, consequently, the position of the inflection point T$_{inf}$ (Figures S3 a-b in the Supplementary Information). As expected, increasing contents of TFA resulted in a decrease of T$_{inf}$ due to the lower degradation temperature of the amide compared to LiPF$_6$ [36,37]. Interestingly, the highest value of T$_{inf}$ was not observed in correspondence of the maximum LiPF$_6$ content (180°C for TFA:LiPF$_6$ 50:50) but for TFA:LiPF$_6$ 80:20 (T$_{inf}$=188°C) confirming once more the extent of the intermolecular interactions, established at the eutectic ratio, that contribute to stabilize the system.
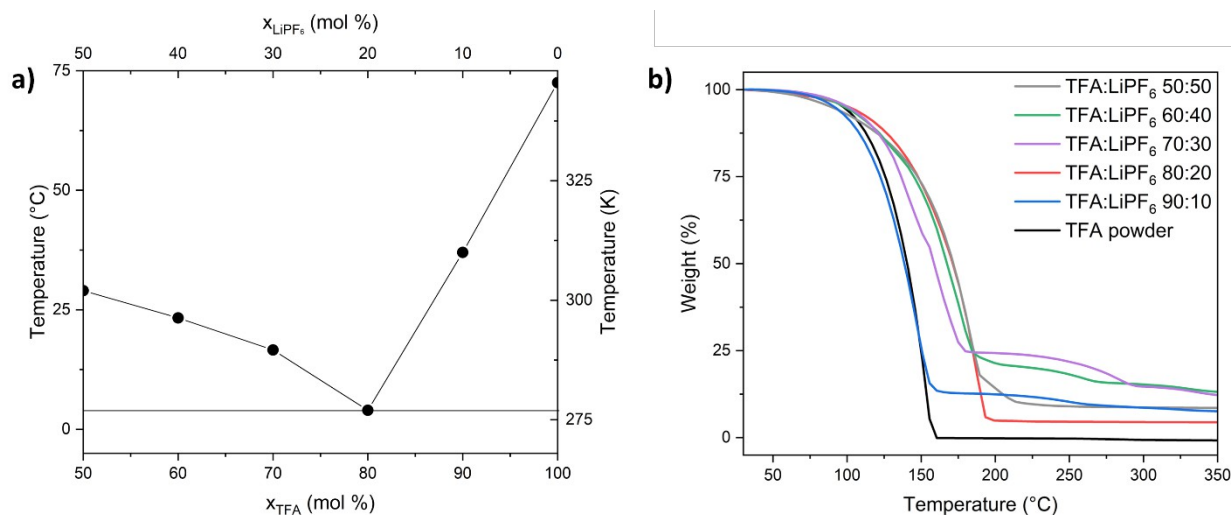
Figure 2: a) Tentative phase diagram of the binary system TFA:LiPF$_6$. b) TGA profile of TFA powder and TFA:LiPF$_6$ DESs performed in N$_2$ atmosphere at a heating rate of 10°C/min.

The ionic conductivity of the different TFA-based DESs at the eutectic composition (Figure 3a) and of the other TFA:LiPF$_6$ compositions were investigated (Figure 3b). Some of the investigated temperatures are below the estimated melting points of Figure 2a, however the solutions under analysis did not show any precipitate because of metastability. Only in the case of the TFA:LiPF$_6$ 90:10 sample, the analysis was not performed because the electrolyte resulted unstable in the low temperature region where a precipitate was observed. For the sake of comparison, the eutectic TFA:TFSI 80:20 solution was prepared, and the results agreed with the literature data [31]. From Figure 3a, however, it is possible to notice the clear improvements on the conductivity imparted by the substitution of LiTFSI with LiPF$_6$: indeed at 25°C the conductivity of the TFA:LiPF$_6$ 80:20 is three times higher than the conductivity of the same composition made with TFSI. The increase of electrical properties of LiPF$_6$-containing solutions compared with those of LiTFSI have already been observed in various solvents such as PC [38] and EC/DMC [39]. The higher conductivity of LiPF$_6$ has been attributed to the higher ionic dissociation in such salt, despite the smaller size and sphericity of the PF$_6$-anion inducing higher viscosity due to a larger solvation sphere compared to the asymmetric and bigger TFSI$^-$. Addition of EC slightly increased the overall conductivity thanks to

the expected reduction of viscosity. Figure 3b shows the dependence of ionic conductivity from the molar ratio of the two components of the DES. As already stated, the best results were obtained using a fixed 80:20 ratio with a room temperature value $\sigma \approx 3.5$ mS cm^{-1}. Consequently, subsequent electrochemical testing was performed only using the solution at the eutectic ratio.
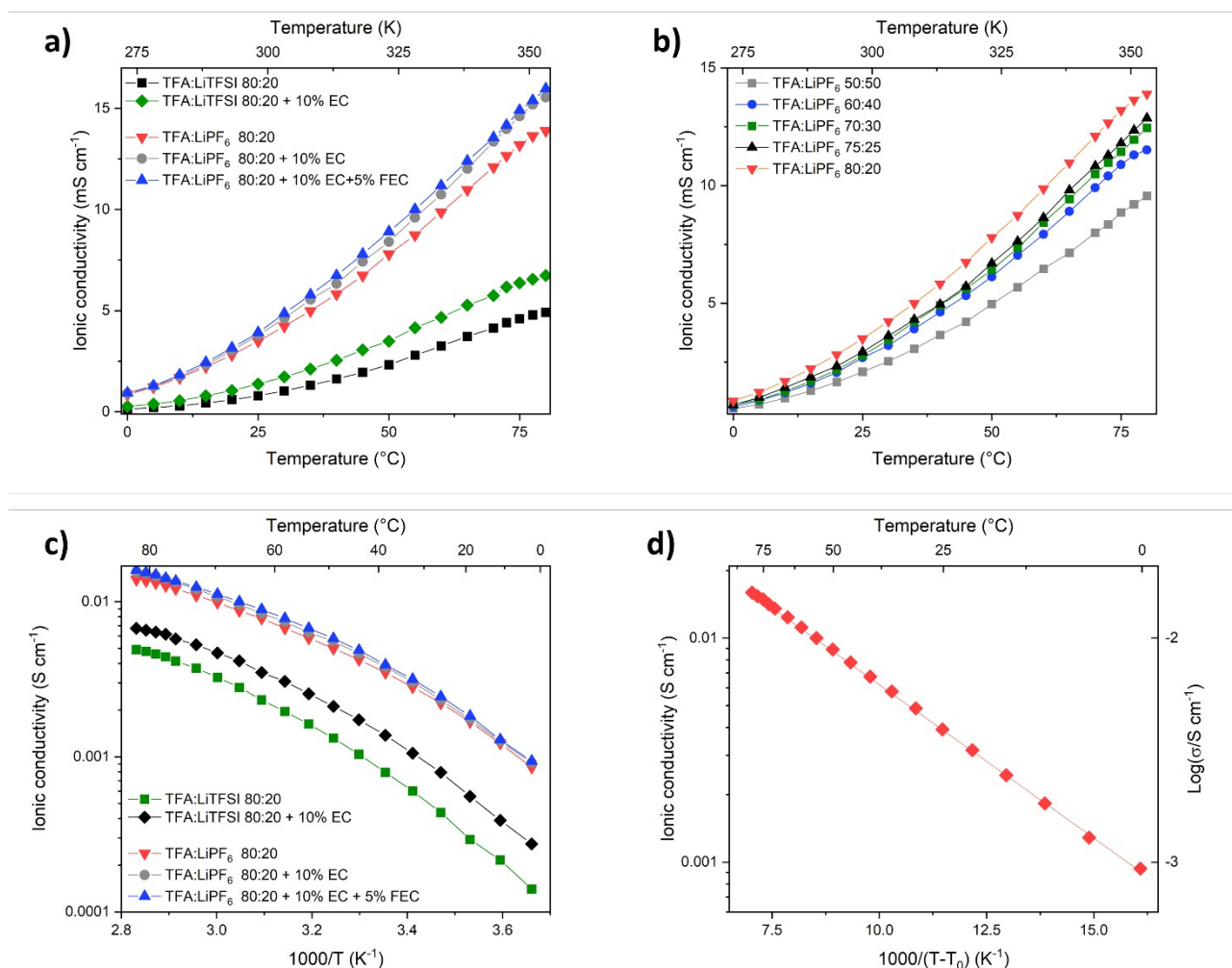

Figure 3: Ionic conductivity of (a) DESs based on different HBA at the eutectic composition, and (b) different molar ratios between TFA and LiPF$_6$. c) Arrhenius plot of TFA-based DESs with LiTFSI and LiPF$_6$. d) VTF plot of TFA-LiPF$_6$ 80:20 +10%EC+5%FEC. Fitting parameters are reported in Table 3.

In the Arrhenius plots (Figure 3c) all the solutions showed a non-linear behaviour, which was successfully fitted with the empirical Vogel-Tammann-Fulcher (VTF) equation:

where B is a pseudo-activation energy expressed in Kelvin and T_0 is a parameter which may be

related to an "ideal" glass transition temperature. A typical best fit is shown in Figure 3d for the

eutectic composition with additives, and the fit results are reported in Table 3 for all the

electrolytes.

Table 3. Electrical properties and VTF best fits of the investigated samples. σ_{Li+}: ionic conductivity at 25°C; σ_0, T_0, and B: VTF fitting parameters; T_g: glass transition temperature determined from DSC analyses.

	σ_{Li+} at 25°c (mS cm^{-1})	σ_0 (S cm^{-1})	T_0 (K)	B (K)	T_g (K)
TFA:LiPF$_6$ 50:50	2.09	0.48	193	476	204
TFA:LiPF$_6$ 60:40	2.69	0.46	202	406	206
TFA:LiPF$_6$ 70:30	2.79	0.49	199	406	206
TFA:LiPF$_6$ 75:25	2.93	0.46	202	395	n.a.
TFA:LiPF$_6$ 80:20	3.49	0.44	206	360	202
TFA:LiPF$_6$ 80:20 +10%EC	3.79	0.47	206	360	n.a.
TFA:LiPF$_6$ 80:20 +10%EC +5%FEC	3.91	0.44	211	325	n.a.

 parameter did not show any clear trend across the composition range, and it is in line with the

calorimetric T_g values obtained by DSC. In contrast, B showed a clear decreasing behavior by

increasing TFA content, es expected from the conductivity data. The addition of 5% FEC has a

beneficial effect, by further decreasing the pseudo-activation energy B.

The Li$^+$ transference number () of the most performing solution (TFA:LiPF$_6$ 80:20 + 10%EC +5% FEC)

was determined using Bruce-Vincent method [40]. The corresponding DC and AC curves are

reported in Figure S4 in the Supplementary Information. The was then obtained using the

formula:

where ΔV is the constant applied potential, I_0 and R_0 are the initial current and the initial interfacial resistance, I_s and R_s the current and the interfacial resistance at the steady state. The estimated Li^+ transference number for the TFA:LiPF$_6$ 80:20 + 10%EC +5% FEC electrolyte was 0.2.

The electrochemical stability of the TFA:LiPF$_6$ 80:20 solutions was then evaluated by CV to estimate both the anodic and the cathodic decomposition potentials. The eutectic composition without carbonate additive was stable up to $\approx$ 4.55 V vs. Li^+/Li, demonstrating its compatibility with most of the cathodic materials for LIBs (Figure S5 in the Supplementary Information). No differences were noticed between the solutions containing only EC and EC+FEC.

Conversely, the TFA:LiPF$_6$ 80:20 DES was unstable at low potentials, presenting an irreversible peak at ca. 1.25 V vs. Li^+/Li which can be attributed to TFA reduction (Figure S6a in the Supplementary Information). In this case, the lithium plating/stripping process shifted in potential and increased in current, probably because of the increased surface area of the freshly formed metallic lithium and of the dynamic SEI formation. Better results were observed for the carbonate containing electrolyte (10%EC and 5% FEC). As shown in Figure S6b in the Supplementary Information, the 1st cycle showed a strong reductive process related both to TFA and FEC degradation (note that the current scale is much lower compared to figure S6a). This phenomenon seems to produce a more stable interface that leads to a stabilization of the peaks related to the Li stripping and plating process.

3.3 Functional characterization

Symmetric Li│DES│Li coin cells were assembled to verify the stripping/plating capability of our DESs and the interfacial stability with respect to Li anode under galvanostatic cycling. In particular, the system containing no additives was unstable and did not permit any noteworthy stable cycling. Conversely, as shown in Figure 4, EC and FEC addition enabled the system to operate stably for

more than 50 hours with a reduced overpotential at a current density of 1 mA cm^{-2} and at a lithium plating capacity of 1 mAh cm^{-2}. In order to understand the reasons for this behavior, we investigated the surface morphology of lithium electrodes after a few cycles of stripping-plating. The images, shown in Figures S7 a-d in the Supporting Information show that the use of additives makes the lithium metal surface much smoother, probably due to the formation of a more stable SEI and the suppression of dendritic growths. These observations are also supported by the EDX investigation (Figure S7 e-f), which shows an important presence of F on the surface of lithium cycled in the absence of carbonates, probably due to the formation of inorganic fluorides (LiF). The presence of unwashed salt can be excluded in the higher resolution images and the absence of the P signal in the spectrum (not shown). Conversely, in the spectrum of the sample cycled in the presence of additives, the C and O signals increase significantly, probably indicating both the presence of LiCO$_3$ and of the organic derivatives produced by the decomposition of carbonates that normally protect the inorganic layer from dissolution.
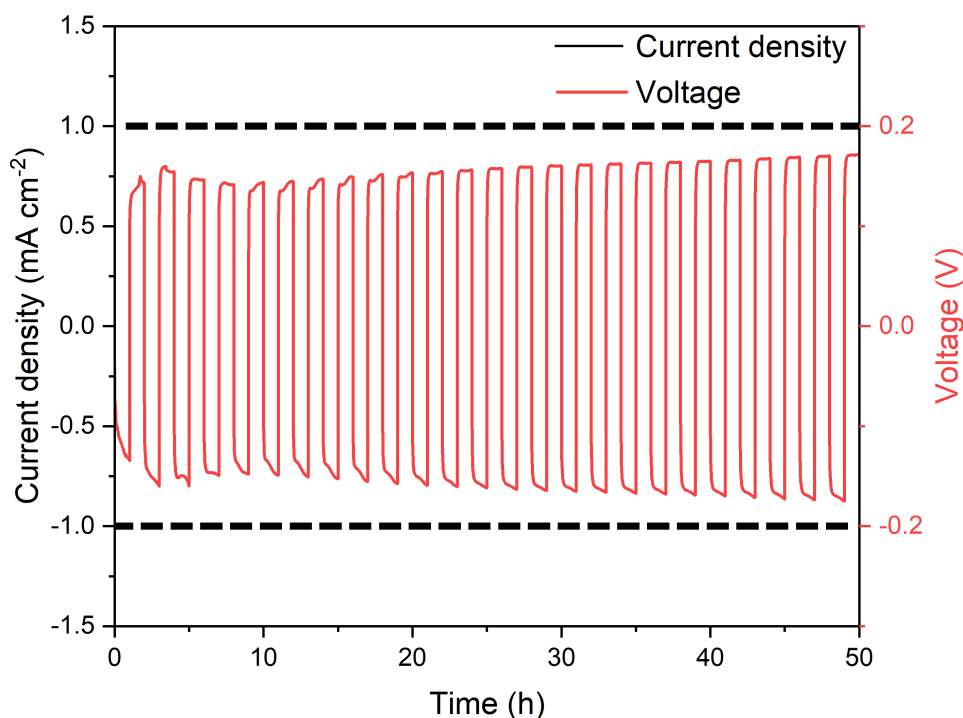

Figure 4: Voltage profile showing the lithium stripping/plating process for a symmetric Li/Li coin cell containing TFA:LiPF$_6$ 80:20+10%EC+5%FEC at a current density of 1 mA cm^{-2} (1 hour for each half cycle).

After having confirmed the compatibility of TFA:LiPF$_6$ 80:20+10%EC+5%FEC with respect to stripping/plating of Li anode, this electrolyte was tested in lithium-metal batteries equipped with different intercalation cathodes to determine its performance during galvanostatic cycling. Galvanostatic cycling measurements with potential limitation (GCPL) were performed on Li│DES│LFP and Li│DES│NMC111 cells using the eutectic composition. In the former case, the DES was formulated both with and without carbonate additives, to further highlight the importance of interface stabilization. LFP-based cells were cycled at C/10 with respect to the cathode mass using cut-off potentials of 4.1 V and 2.4 V vs. Li$^+$/Li. Figure S8 of the Supplementary Information reported the voltage profile of the cell employing TFA:LiPF$_6$ 80:20 with no additives, and the relative efficiency vs. cycle number. The first cycle discharge specific capacity was 75 mAh g^{-1}. This value decreased to 50 mAh g^{-1} after 20 cycles, after which the cell underwent a dramatic decrease of performances. It was clear that the electrolyte is not able to operate in contact with Li metal, due to the impossibility of forming a stable anodic SEI.
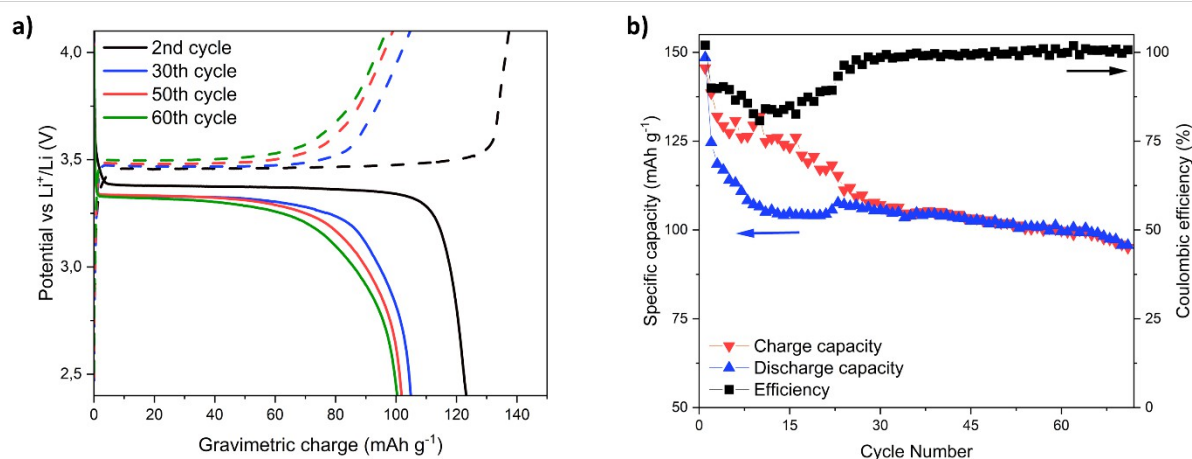

Figure 5: a) Charge discharge profile at C/10 of a Li|DES|LFP three-electrode Swagelok cell employing TFA:LiPF$_6$ 80:20 + 10%EC + 5%FEC as the electrolyte and (b) corresponding cycle performance.

Conversely, after some stabilization cycles required for the formation of SEI, the electrolyte with the additives (10% EC, 5% FEC) operated stably for more than 70 cycles delivering specific capacity

of about 100 mAh g^{-1} with a reduced overpotential (Figure 5a). The coulombic efficiency (CE) strongly improved upon cycling, reaching an average value of 99.1% in the last 15 cycles (Figure 5b).

The high- voltage cathodic material NMC111 was also tested in the potential range 2.7 V - 4.3 V vs. Li$^+$/Li at C/10. However, this preliminary testing yielded results not comparable to the ones achieved using LFP since, despite of additives addition, as continuous capacity fading was observed along the first 40 cycles (see Figure 6a,b).
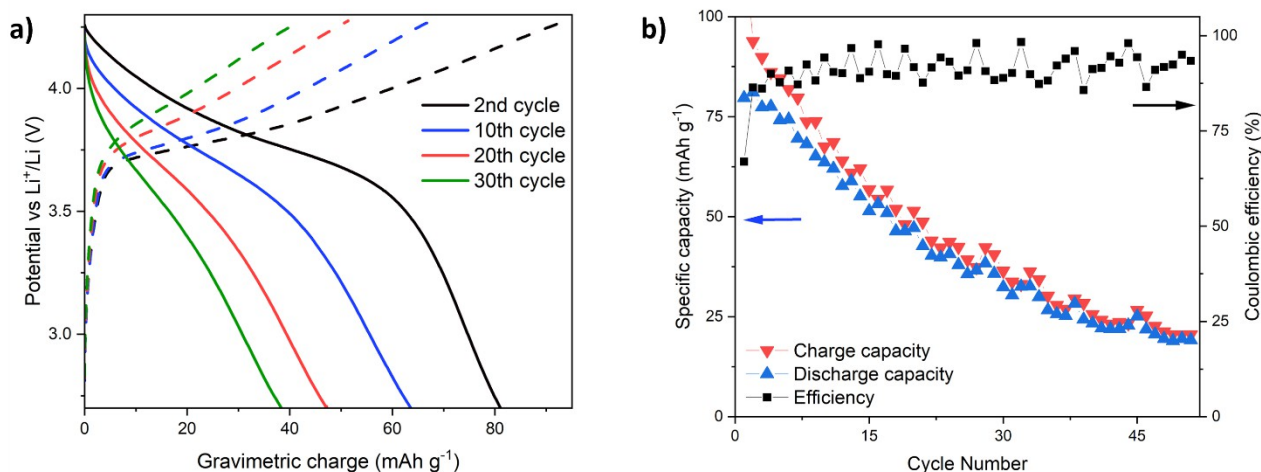

Figure 6: a) Charge discharge profile of a Li|DES|NMC111 three electrode Swagelok cell employing TFA:LiPF$_6$ 80:20 + 10%EC + 5%FEC as electrolyte and (b) corresponding cycle performance.

To understand the difference between the two active materials and highlight any cathode dissolution problems, we performed two experiments in which the LFP and NMC powders were left in contact with DES 80:20 for a certain period of time. To facilitate any etching, the amount of active material was relatively small (10 mg) compared to that of the solvent (500 mg). After one week, the solution was filtered and analyzed with ICP to determine the concentrations of Fe in the first sample and of Ni, Mn and Co in the second. The results of the two experiments were very different: in the case of Fe, the quantity determined in solution was 3% of that initially present in

the 10 mg of LFP, while for NMC the quantities solubilized in the solvent were respectively 19, 20 and 11% for Ni, Mn, and Co. This demonstrates that the instability seen in Figure 6 is due to the solubility of NMC, which should therefore be protected at the surface.

Although the Li|DES|NMC111 cell is not optimized and its performance must be improved, this more critical configuration was used during ARC testing to demonstrate the improved safety imparted by to the use of DES. The results are shown in Figure 7 and their qualitative analysis allows us to appreciate the improved thermal stability of the DES electrolyte even in the presence of cyclic carbonates. In fact, both the cells showed the onset temperature of a first degradation reaction between 100 and 120°C due to the decomposition of SEIs. From here on, both cells began to self-heat, up to a temperature of 150°C at which cathode decomposition occurred [41]. Following this, the behavior of the two cells is completely different. The cell with the commercial electrolyte showed an exponential increase in temperature that quickly caused thermal runaway (the measurement was still stopped at 250°C), whereas in the cell with DES the temperature increased much more gradually until it stabilized at 195°C. To reach the cut-off temperature, the system had to be reheated externally, and the final temperature was still reached with temperature gradients < 0.05 °C min^{-1}.
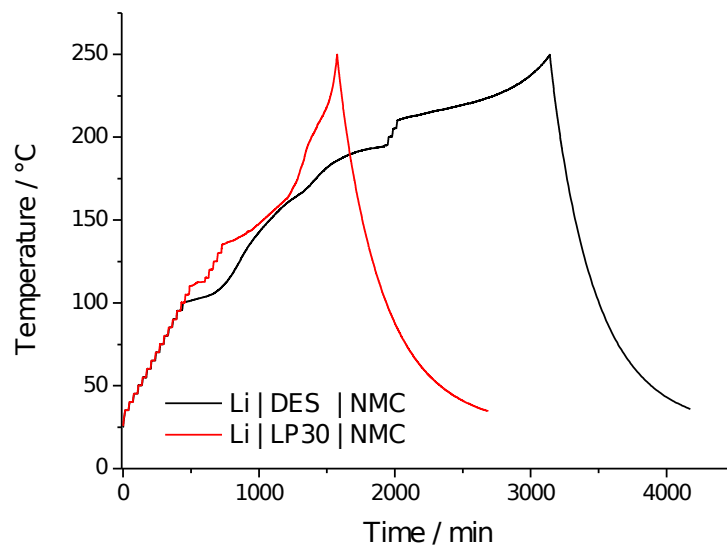
Figure 7: Temperature vs. time profiles of ARC measurements for the Li| TFA:LiPF$_6$ 80:20 + 10%EC + 5%FEC |NMC (black curve) and the Li| LP30 |NMC (red curve) coin cell.

4 Conclusions

The physico-chemical and electrochemical properties of TFA:LiPF$_6$ DESs are attractive for future developments as electrolytes in rechargeable lithium-ion batteries. Indeed, the eutectic composition (TFA:LFP$_6$ 80:20) shows good conductivity at room temperature (3.5 mS cm^{-2}), which can be further improved with the addition of cyclic carbonates that can also have a beneficial effect in terms of safety. The presence of these additives is also beneficial to mitigate the cathodic instability of TFA, indeed we have demonstrated that EC and FEC are able to form a more stable SEI. The electrolyte performance in batteries equipped with LFP cathode was encouraging, while those with high-voltage active material still need to be optimized, chiefly by working on the stability of the cathode interface. In the former case, the cell was able to operate for 70 cycles with a specific capacity higher than 100 mAh g^{-1}. In the latter, however, a net increasing of the thermal stability of the cell was demonstrated by ARC tests.

Appendix A. Supplementary data

Results of flammability test, DSC profiles, analysis of TGA first derivatives, Bruce-Vincent method, anodic and cathodic stability, morphological changes of Li anodes upon cycling with and without additives, and performance of a Li│DES│LFP cell without additives can be found in the Supporting Information.

REFERENCES:

[1]   Z.P. Cano, D. Banham, S. Ye, A. Hintennach, J. Lu, M. Fowler, Z. Chen, Batteries and fuel cells for emerging electric vehicle markets, Nat Energy. 3 (2018) 279–289. https://doi.org/10.1038/s41560-018-0108-1.

[2]   M. Zhang, D.A. Kitchaev, Z. Lebens-Higgins, J. Vinckeviciute, M. Zuba, P.J. Reeves, C.P. Grey, M.S. Whittingham, L.F.J. Piper, A. van der Ven, Y.S. Meng, Pushing the limit of 3d transition metal-based layered oxides that use both cation and anion redox for energy storage, Nat Rev Mater. (2022). https://doi.org/10.1038/s41578-022-00416-1.

[3]   A. Eftekhari, Lithium Batteries for Electric Vehicles: From Economy to Research Strategy, ACS Sustain Chem Eng. 7 (2019) 5602–5613. https://doi.org/10.1021/acssuschemeng.8b01494.

[4]   J. Neubauer, E. Wood, The impact of range anxiety and home, workplace, and public charging infrastructure on simulated battery electric vehicle lifetime utility, J Power Sources. 257 (2014) 12–20. https://doi.org/10.1016/j.jpowsour.2014.01.075.

[5]   M.S.E. Houache, C.-H. Yim, Z. Karkar, Y. Abu-Lebdeh, On the Current and Future Outlook of Battery Chemistries for Electric Vehicles—Mini Review, Batteries. 8 (2022) 70. https://doi.org/10.3390/batteries8070070.

[6]   Z. Ye, L. Qiu, W. Yang, Z. Wu, Y. Liu, G. Wang, Y. Song, B. Zhong, X. Guo, Nickel-Rich Layered Cathode Materials for Lithium-Ion Batteries, Chemistry - A European Journal. 27 (2021) 4249–4269. https://doi.org/10.1002/chem.202003987.

[7]   M. Fichtner, K. Edström, E. Ayerbe, M. Berecibar, A. Bhowmik, I.E. Castelli, S. Clark, R. Dominko, M. Erakca, A.A. Franco, A. Grimaud, B. Horstmann, A. Latz, H. Lorrmann, M. Meeus, R. Narayan, F. Pammer, J. Ruhland, H. Stein, T. Vegge, M. Weil, Rechargeable Batteries of the Future—The State of the Art from a BATTERY 2030+ Perspective, Adv Energy Mater. 12 (2022). https://doi.org/10.1002/aenm.202102904.

[8]   M. Ierides, R. del Valle, D. Fernandez, L. Bax, P. Jacques, F. Stassin, M. Meeus, Advanced Materials for Clean and Sustainable Energy and Mobility, 2019.

[9]   C. Arbizzani, G. Gabrielli, M. Mastragostino, Thermal stability and flammability of electrolytes for lithium-ion batteries, J Power Sources. 196 (2011) 4801–4805. https://doi.org/10.1016/j.jpowsour.2011.01.068.

[10]   Q. Wang, P. Ping, X. Zhao, G. Chu, J. Sun, C. Chen, Thermal runaway caused fire and explosion of lithium ion battery, J Power Sources. 208 (2012) 210–224. https://doi.org/10.1016/j.jpowsour.2012.02.038.

[11]   E. Quartarone, P. Mustarelli, Emerging Trends in the Design of Electrolytes for Lithium and Post-Lithium Batteries, J Electrochem Soc. 167 (2020) 050508. https://doi.org/10.1149/1945-7111/ab63c4.

[12]   R. Gond, W. van Ekeren, R. Mogensen, A.J. Naylor, R. Younesi, Non-flammable liquid electrolytes for safe batteries, Mater Horiz. 8 (2021) 2913–2928. https://doi.org/10.1039/d1mh00748c.

[13]   J. Wu, Q. Liang, X. Yu, L. Qiu-Feng, L. Ma, X. Qin, G. Chen, B. Li, Deep Eutectic Solvents for Boosting Electrochemical Energy Storage and Conversion: A Review and Perspective, Adv Funct Mater. 31 (2021). https://doi.org/10.1002/adfm.202011102.

[14]   S. Yan, Y. Wang, T. Chen, Z. Gan, S. Chen, Y. Liu, S. Zhang, Regulated interfacial stability by coordinating ionic liquids with fluorinated solvent for high voltage and safety batteries, J Power Sources. 491 (2021). https://doi.org/10.1016/j.jpowsour.2021.229603.

[15]   X. Tang, S. Lv, K. Jiang, G. Zhou, X. Liu, Recent development of ionic liquid-based electrolytes in lithium-ion batteries, J Power Sources. 542 (2022). https://doi.org/10.1016/j.jpowsour.2022.231792.

[16]   D.R. MacFarlane, M. Forsyth, P.C. Howlett, M. Kar, S. Passerini, J.M. Pringle, H. Ohno, M. Watanabe, F. Yan, W. Zheng, S. Zhang, J. Zhang, Ionic liquids and their solid-state analogues as materials for energy generation and storage, Nat Rev Mater. 1 (2016). https://doi.org/10.1038/natrevmats.2015.5.

[17]   I. Osada, H. de Vries, B. Scrosati, S. Passerini, Polymerelektrolyte auf Basis ionischer Flüssigkeiten für Batterieanwendungen, Angewandte Chemie. 128 (2016) 510–523. https://doi.org/10.1002/ange.201504971.

[18]   M. Galiński, A. Lewandowski, I. Stepniak, Ionic liquids as electrolytes, Electrochim Acta. 51 (2006) 5567–5580. https://doi.org/10.1016/j.electacta.2006.03.016.

[19]   E.L. Smith, A.P. Abbott, K.S. Ryder, Deep Eutectic Solvents (DESs) and Their Applications, Chem Rev. 114 (2014) 11060–11082. https://doi.org/10.1021/cr300162p.

[20]   T. el Achkar, H. Greige-Gerges, S. Fourmentin, Basics and properties of deep eutectic solvents: a review, Environ Chem Lett. 19 (2021) 3397–3408. https://doi.org/10.1007/s10311-021-01225-8.

[21]   H. Ogawa, H. Mori, Lithium salt/amide-based deep eutectic electrolytes for lithium-ion batteries: electrochemical, thermal and computational study, Physical Chemistry Chemical Physics. 22 (2020) 8853–8863. https://doi.org/10.1039/d0cp01255f.

[22] C.R. Gregg, O.J. Tejeda, L.F. Spencer, A.J. Calderon, D. v. Bourassa, J.D. Starkey, C.W. Starkey, Impacts of Increasing Additions of Choline Chloride on Growth Performance and Carcass Characteristics of Broiler Chickens Reared to 66 Days of Age, Animals. 12 (2022). https://doi.org/10.3390/ani12141808.

[23] B.B. Hansen, S. Spittle, B. Chen, D. Poe, Y. Zhang, J.M. Klein, A. Horton, L. Adhikari, T. Zelovich, B.W. Doherty, B. Gurkan, E.J. Maginn, A. Ragauskas, M. Dadmun, T.A. Zawodzinski, G.A. Baker, M.E. Tuckerman, R.F. Savinell, J.R. Sangoro, Deep Eutectic Solvents: A Review of Fundamentals and Applications, Chem Rev. (2021). https://doi.org/10.1021/acs.chemrev.0c00385.

[24] A.P. Abbott, G. Capper, D.L. Davies, R.K. Rasheed, V. Tambyrajah, Novel solvent properties of choline chloride/urea mixtures, Chemical Communications. (2003) 70–71. https://doi.org/10.1039/b210714g.

[25] A. Boisset, S. Menne, J. Jacquemin, A. Balducci, M. Anouti, Deep eutectic solvents based on N-methylacetamide and a lithium salt as suitable electrolytes for lithium-ion batteries, Physical Chemistry Chemical Physics. 15 (2013) 20054–20063. https://doi.org/10.1039/c3cp53406e.

[26] O.E. Geiculescu, D.D. Desmarteau, S.E. Creager, O. Haik, D. Hirshberg, Y. Shilina, E. Zinigrad, M.D. Levi, D. Aurbach, I.C. Halalay, Novel binary deep eutectic electrolytes for rechargeable Li-ion batteries based on mixtures of alkyl sulfonamides and lithium perfluoroalkylsulfonimide salts, J Power Sources. 307 (2016) 519–525. https://doi.org/10.1016/j.jpowsour.2015.11.072.

[27] L. Millia, V. Dall'Asta, C. Ferrara, V. Berbenni, E. Quartarone, F.M. Perna, V. Capriati, P. Mustarelli, Bio-inspired choline chloride-based deep eutectic solvents as electrolytes for lithium-ion batteries, Solid State Ion. 323 (2018) 44–48. https://doi.org/10.1016/j.ssi.2018.05.016.

[28] B. Joos, T. Vranken, W. Marchal, M. Safari, M.K. van Bael, A.T. Hardy, Eutectogels: A New Class of Solid Composite Electrolytes for Li/Li-Ion Batteries, Chemistry of Materials. 30 (2018) 655–662. https://doi.org/10.1021/acs.chemmater.7b03736.

[29] C. Wang, H. Zhang, S. Dong, Z. Hu, R. Hu, Z. Guo, T. Wang, G. Cui, L. Chen, High Polymerization Conversion and Stable High-Voltage Chemistry Underpinning an in Situ Formed Solid Electrolyte, Chemistry of Materials. 32 (2020) 9167–9175. https://doi.org/10.1021/acs.chemmater.0c02481.

[30] P. Jaumaux, Q. Liu, D. Zhou, X. Xu, T. Wang, Y. Wang, F. Kang, B. Li, G. Wang, Deep-Eutectic-Solvent-Based Self-Healing Polymer Electrolyte for Safe and Long-Life Lithium-Metal Batteries, Angewandte Chemie - International Edition. 59 (2020) 9134–9142. https://doi.org/10.1002/anie.202001793.

[31] T.T.A. Dinh, T.T.K. Huynh, L.T.M. Le, T.T.T. Truong, O.H. Nguyen, K.T.T. Tran, M. v. Tran, P.H. Tran, W. Kaveevivitchai, P.M.L. Le, Deep Eutectic Solvent Based on Lithium Bis[(trifluoromethyl)sulfonyl] Imide (LiTFSI) and 2,2,2-Trifluoroacetamide (TFA) as a Promising Electrolyte for a High Voltage Lithium-Ion Battery with a LiMn2O4Cathode, ACS Omega. 5 (2020) 23843–23853. https://doi.org/10.1021/acsomega.0c03099.

[32] E. Peled, The Electrochemical Behavior of Alkali and Alkaline Earth Metals in Nonaqueous Battery Systems-The Solid Electrolyte Interphase Model, J. Electrochem. Soc. 126 (1979) 2047.

[33] G.G. Eshetu, S. Grugeon, S. Laruelle, S. Boyanov, A. Lecocq, J.P. Bertrand, G. Marlair, In-depth safety-focused analysis of solvents used in electrolytes for large scale lithium ion batteries, Physical Chemistry Chemical Physics. 15 (2013) 9145–9155. https://doi.org/10.1039/c3cp51315g.

[34] P. Mustarelli, C. Tomasi, M. Villa, Heat Capacities of Thermally Treated Na 2 0-3B 2 0 3 Glasses Above and Below T g, Z. Naturforsch. 51 (1996) 187–191.

[35] P. Stigliano, C. Ferrara, N. Pianta, A. Gentile, L. Mezzomo, R. Lorenzi, V. Berbenni, R. Ruffo, G.B. Appetecchi, P. Mustarelli, Physicochemical properties of Pyr13TFSI-NaTFSI electrolyte for sodium batteries, Electrochim Acta. 412 (2022). https://doi.org/10.1016/j.electacta.2022.140123.

[36]   H. Yang, G. v. Zhuang, P.N. Ross, Thermal stability of LiPF6 salt and Li-ion battery electrolytes containing LiPF6, J Power Sources. 161 (2006) 573–579. https://doi.org/10.1016/j.jpowsour.2006.03.058.

[37]   E. Zinigrad, L. Larush-Asraf, J.S. Gnanaraj, M. Sprecher, D. Aurbach, On the thermal stability of LiPF6, Thermochim Acta. 438 (2005) 184–191. https://doi.org/10.1016/j.tca.2005.09.006.

[38]   T. Nishida, K. Nishikawa, Y. Fukunaka, Diffusivity Measurement of LiPF6, LiTFSI, LiBF4 in PC, ECS Trans. 6 (2008) 1–14. https://doi.org/10.1149/1.2831921.

[39]   M. Dahbi, F. Ghamouss, F. Tran-Van, D. Lemordant, M. Anouti, Comparative study of EC/DMC LiTFSI and LiPF6 electrolytes for electrochemical storage, J Power Sources. 196 (2011) 9743–9750. https://doi.org/10.1016/j.jpowsour.2011.07.071.

[40]   P.G. Bruce, J. Evans, C.A. Vincent, Conductivity and transference number measurements on polymer electrolytes, Solid State Ion. 28–30 (1988) 918–922. https://doi.org/10.1016/0167-2738(88)90304-9.

[41]   Q. Wang, B. Mao, S.I. Stoliarov, J. Sun, A review of lithium ion battery failure mechanisms and fire prevention strategies, Prog Energy Combust Sci. 73 (2019) 95–131. https://doi.org/10.1016/j.pecs.2019.03.002.